ARTICLE

# Ultrafast Dynamics of Water Molecules Excited to Electronic $\tilde{F}$ States: A Time-Resolved Photoelectron Spectroscopy Study[†]

Dong-yuan Yang[a,b‡], Yan-jun Min[a,b‡], Zhen Chen[a,b‡], Zhi-gang He[a], Zhi-chao Chen[a], Kai-jun Yuan[a], Dong-xu Dai[a], Guo-rong Wu[a*], Xue-ming Yang[a]

*a. State Key Laboratory of Molecular Reaction Dynamics, Dalian Institute of Chemical Physics, Dalian 116023, China*
*b. University of Chinese Academy of Sciences, Beijing 100049, China*

(Dated: Received on November 4, 2018; Accepted on January 3, 2019)

The ultrafast dynamics of water molecules excited to the two $\tilde{F}$ states is studied by combining two-photon excitation and time-resolved photoelectron imaging techniques. The lifetimes of the $\tilde{F}^1A_1$ and $\tilde{F}^1B_1$ states of $H_2O$ ($D_2O$) were derived to be 1.0±0.3 (1.9±0.4) and 10±3 (30±10) ps, respectively. We propose that the $\tilde{F}^1A_1$ state mainly decays through the $\tilde{D}$ state, due to the nonadiabatic coupling between them, while the $\tilde{F}^1B_1$ state decays through the $\tilde{F}^1A_1$ state via Coriolis interaction.

**Key words:** Photoelectron spectrum, Pump/probe, Femtosecond time-resolved sprctra

## I. INTRODUCTION

Photochemistry of water in the gas phase is one of the most important, yet challenging topic in molecular reaction dynamics. It also serves as an ideal model system to study complicated excited-state dynamics of polyatomic molecules. Excited-state dynamics of water molecules has been intensively studied, both experimentally and theoretically, for more than four decades, rich information has been obtained from various studies, such as absorption spectra [1], resonance-enhanced multiphoton ionization (REMPI) spectra [2], OH product fluorescence excitation spectra [3], H product action spectra [4] and photodissociation dynamics [5, 6], time-resolved excited-state dynamics [7, 8], *etc.*

Among these studies, most focus on the four lowest singlet excited states, $\tilde{A}^1B_1$, $\tilde{B}^1A_1$, $\tilde{C}^1B_1$, and $\tilde{D}^1A_1$ states. Excitation in the longest wavelength vacuum ultraviolet (VUV) absorption band of water around 150−200 nm leads to excitation of the $\tilde{A}$ state which is a prototype of direct dissociation with a lifetime around 20 fs [9–11]. The $\tilde{B}^1A_1$ state, corresponding to the second absorption band centered around 128 nm, exhibits very complicated and interesting dynamics [12–18]. Adiabatic dissociation on the $\tilde{B}$ state potential energy surface (PES) leads to H atom and first excited electronic state $OH(\tilde{A}^2\Sigma^+)$ radical. However, the main dissociation channel of the $\tilde{B}$ state is predissociation through the $\tilde{A}$ and $\tilde{X}$ states, generating H atom and the ground state $OH(\tilde{X}^2\Pi)$ radical. There are two conical intersections (CI) between the $\tilde{B}$ and $\tilde{X}$ states, both linear and with H−O−H and O−H−H geometry, respectively, facilitating a very efficient nonadiabatic transition from the $\tilde{B}$ to the $\tilde{X}$ state. Wavepacket on the $\tilde{B}$ state PES evolving to $H+OH(\tilde{X}^2\Pi)$ products through both CIs and quantum interference has been observed, manifesting itself with oscillations in the even-odd rotational state population of OH products [19]. The first rotationally resolved absorption band is the transition to the $\tilde{C}$ state located around 124 nm [1, 2, 20, 21]. The $\tilde{C}$ state was found to be predissociative with a lifetime of the order of 1 ps, but showed a clear dependence on $\langle {J_a}^2 \rangle$ (the expectation value of the square of the rotational angular momentum about the molecular $a$-axis): with an increase of $\langle {J_a}^2 \rangle$, the lifetime of the $\tilde{C}$ state rapidly decreases [2, 4, 7, 21–23]. In one of our recent studies, an accidental resonance mediated predissociation pathway for the first bending mode excited state in the $\tilde{C}$ state of $H_2O$ was also revealed [8]. The next electronic state is the $\tilde{D}$ state which is strongly predissociated by the $\tilde{B}$ state [24]. The wavepacket initially excited to the $\tilde{D}$ state evolves promptly to the $\tilde{B}$ state PES, and then following the photodissociation dynamics on the $\tilde{B}$ state PES, resulting in a similar internal state and angular distributions of the OH products with those from the $\tilde{B}$ state when it is directly excited.

The study of dynamics of $H_2O$ molecules excited to higher Rydberg states, such as the $\tilde{E}$ and $\tilde{F}$ states, is rare, due to the lack of the tunable and intense VUV radiation source. Recently, the photodissociation dynamics of $H_2O$ excited to the $\tilde{F}$ states at 111.5 nm has

[†]Dedicated to Professor Kopin Liu on the occasion of his 70th birthday.
[‡]These authors contributed to this work equally.
*Author to whom correspondence should be addressed. E-mail: wugr@dicp.ac.cn

 

been studied by Yuan and coworkers using a tunable VUV free electron laser (FEL) facility (Dalian Coherent Light Source, DCLS) and the H-atom Rydberg "tagging" time-of-flight (TOF) technique [25]. The internal state and angular distributions of the H+OH products were derived and the possible dissociation mechanisms were discussed.

In this paper, we present a fs time-resolved study on the ultrafast dynamics of water molecules excited to the $\tilde{F}$ states, by combining two-photon excitation and time-resolved photoelectron imaging (TRPEI) techniques. The lifetimes of the $\tilde{F}$ states are measured and the decay dynamics is discussed in detail.

## II. EXPERIMENTS

The experiment was carried out in a similar way to that described in Ref.[8], on a velocity map imaging (VMI) spectrometer [26]. The pump and probe laser pulses were obtained from a fully integrated Ti:Sapphire oscillator/regenerative amplifier system (<50 fs, 800 nm, 3.8 mJ and 1 kHz, Coherent, Libra-HE). There were two optical parametric amplifiers (OPA, Coherent, OperA Solo), each pumped by a fraction (1.3 mJ per pulse) of the fundamental output of the amplifier. The probe laser pulse was directly obtained from one of the OPAs and fixed at 335.5 nm (∼3 mJ per pulse). For the pump laser pulses (223.0 and 225.6 nm for $H_2O$ and 222.6 nm for $D_2O$, ∼1.5 mJ per pulse), the output of the other OPA (around 500 nm, >20 mJ per pulse) was mixed with a 400 nm laser beam (∼50 mJ per pulse) using an $\beta$-BBO crystal (0.15 mm), which itself was the doubling of a fraction (∼300 mJ per pulse) of the amplifier fundamental output using another $\beta$-BBO crystal (0.1 mm). The bandwidth of the pump pulses was about 170 $cm^{-1}$ (FWHM).

The pump and probe laser pulses were combined collinearly by a dichroic mirror without further compression, and then focused using an $f/75$ lens to intersect a seeded water molecular beam in the interaction region of the VMI spectrometer. The $H_2O$ and $D_2O$ molecular beams were generated by bubbling He of ∼4 bar through the $H_2O$ or $D_2O$ sample at room temperature using an Even-Lavie pulsed valve operated at 1 kHz. Both the pump and probe pulses were linearly polarized and the polarization direction was parallel to the micro channel plate (MCP) detector. Time delays between pump and probe pulses were scanned using a computer-controlled stepper motor which was located upstream of the first OPA to change the delay of input fundamental. Photoelectron images arising from the pump and the probe laser alone were also recorded. The sum of the single color photoelectron images was subtracted in order to correct for background photoelectrons generated from single color multiphoton ionizations. The 2D photoelectron image was transferred to the 3D distribution using the polar basis function expansion method [27]. The time-dependent photoelectron 3D distributions were further integrated along the recoiling angle to derive the kinetic energy distributions of the photoelectron, *i.e.*, time-resolved photoelectron spectra (TRPES).

Electron kinetic energy calibration was achieved using multi-photon ionization of Xe atom. This also served to measure the cross-correlation (*i.e.*, instrumental response function, IRF) between the pump and the probe laser pulses. At pump wavelengths employed here, resonance-enhancement in the multiphoton ionization of Xe was observed which prevented a reliable determination of the cross-correlation. Therefore, the pump pulse was tuned to a slightly longer wavelength to avoid the resonant transition lines in Xe. The time delay-dependent curve of the electron yield was fitted, based on the approximation that both pump and probe laser pulses have a Gaussian profile. It has to be noted here that only photoelectron was generated by absorption of two pump photons and a single probe photon was taken into account in this analysis, thanks to the capability of VMI technique in differentially analyzing the outgoing photoelectron as a function of delay with respect to kinetic energy. The derived $2+1'$ IRF was about 150±5 fs (FWHM), and it was used as an approximation to the true IRF and varied in a small range in the fitting of the photoelectron transients to find a best fit (least squares) and estimate the confidence intervals of the derived time constants. The time-zero overlap and molecular beam condition were checked before and after the TRPES measurement to make sure there was no severe drift of the time-zero during measurement.

## III. RESULTS AND DISCUSSION

### A. Experimental results and data analysis

Water molecules were excited into the $\tilde{F}$ states by two-photon absorption whereupon another delayed laser pulse probed the excited state water molecules via one-photon ionization (FIG. 1). FIG. 2 (a) shows the TRPES data of $H_2O$ at pump wavelength of 223.0 nm. The TRPES data are mainly comprised of three features: a diffuse and strong feature (labeled as feature I in FIG. 2(a)) around time-zero, showing no or a very fast decay dynamics; a single sharp, strong peak (feature II) centered at 2.2 eV, showing a ps decay dynamics; and a weak, diffuse feature (feature III) over the kinetic energy range from 0.8 eV to 1.8 eV with a dynamics shorter than that of feature II. In the following, we first analyze and identify the sources of these features in detail.

By systematically changing the pump and probe wavelengths, it was shown that feature I includes two different contributions, both resulted from a two-color three-photon ionization process. The first contribution, corresponding to the photoelectron around 0.2 eV, is

DOI:10.1063/1674-0068/cjcp1811243 

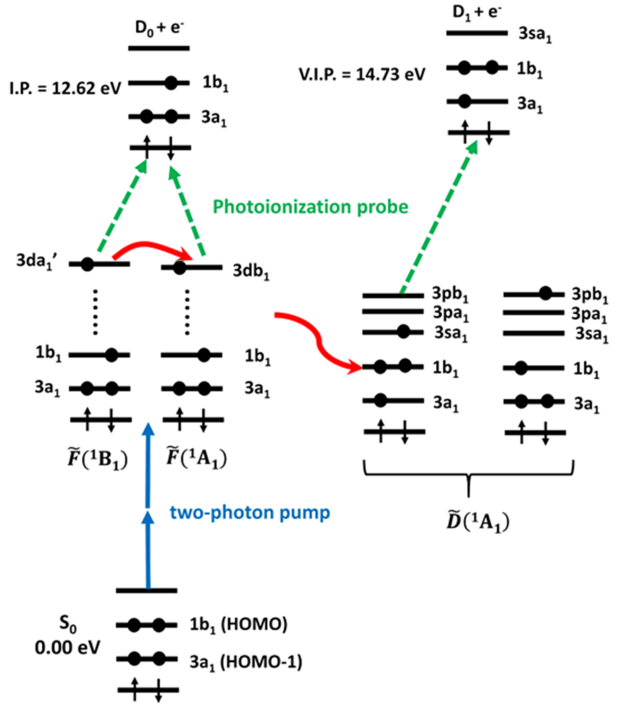


FIG. 1 Schematic view of the pump and probe schemes used in the present experiment and the proposed decay mechanisms of the $\tilde{F}$ states.

associated with a two-probe-photon excitation and one-pump-photon ionization process. Two probe-photons (335.5 nm) correspond to an energy of 7.39 eV. $H_2O$ is excited to the $\tilde{A}$ state by two probe photons and ionized to the ground state ($D_0$) state of $H_2O^+$ by absorbing another pump photon (223.0 nm). The energetic limit of photoelectron from this process is 0.33 eV, calculated using the first photoionization potential of 12.62 eV [28], consistent with the experimental observation. The $\tilde{A}$ state is a prototype of direct dissociation with a lifetime around 20 fs [9–11], rendering to a very fast decay of the corresponding photoelectrons. Photoelectrons of feature I above 0.6 eV arise from another process: one pump-photon plus one probe-photon excitation and one pump-photon ionization. The energy of one pump-photon and one probe-photon is 9.26 eV and corresponds to the excitation of the $\tilde{B}$ state. The $\tilde{B}$ state has a combination of electronic configurations of $3pb_1 \leftarrow 1b_1$ and $3sa_1 \leftarrow 3a_1$, and therefore is associated to both $D_0$ and $D_1$ states of $H_2O^+$ upon photoionization [29, 30]. Further, one of the dissociation channels of the $\tilde{B}$ state is the ultrafast predissociation through the $\tilde{A}$ state [12–18]. The latter mainly corresponds to the ground state ($D_0$) of $H_2O^+$ upon photoionization [30]. The $\tilde{A}$ state is repulsive along the antisymmetric stretching ($\nu_3$) coordinate and would have a broad Franck-Condon (FC) progression along the antisymmetric stretching coordinate upon photoionization, consistent with the experimental results [31]. The kinetic energy distribution of photoelectron of feature I above 0.6 eV is converted into the binding energy distribution, by assuming a process involving two pump photons and one probe photon (FIG. 2(c)). The experimental results at another two pump wavelengths are also included. It is clear that the four peaks can be readily assigned to the four different vibrational states of $D_0$ with $\nu_3$=0−3, further consolidating the assignments of feature I proposed above.

In FIG. 2 (d) and (e), the time delay dependences of feature II (integrated over 2.08−2.28 eV) and III (integrated over 0.80−1.80 eV) are shown. A least-squares method was employed to fit these time delay dependent curves in order to extract more detailed dynamics information. The kinetic model used involves a convolution of the following expression:

$$\text{for } t \geq 0, \quad S(t) = 1 + \sum_{i=1}^{n} A_i \exp\left(-\frac{t}{\tau_i}\right) \qquad (1)$$

$$\text{for } t < 0, \quad S(t) = 0$$

with the IRF which was determined separately. Here, $S(t)$ represents the total time delay-dependent curve, and $A_i \exp\left(-\frac{t}{\tau_i}\right)$ is the contribution with a lifetime and amplitude of $\tau_i$ and $A_i$, respectively. IRF stands for the contribution from feature I which shows dynamics with a time constant much smaller than IRF and can be very well represented by IRF. In the fit, time-zero varied in the range of the experimentally measured time-zero drift and IRF was also varied in the range of their uncertainties to obtain the best fit. This analysis also served to estimate the confidence intervals of these time constants. The derived time constants, together with the corresponding curves for each component are also presented in FIG. 2 (d) and (e).

There are two components derived for the feature II, with a lifetime of 1.0±0.3 and 10±3 ps, respectively. According to the absorption spectrum of water, they are assigned to the $\tilde{F}^1B_1$ and $\tilde{F}^1A_1$ states [20, 32]. Both $\tilde{F}$ states are of Rydberg character with an electron from the highest occupied molecular orbital (HOMO) excited to $3da_1'$, and $3db_1$, respectively, and as such they may be expected to possess a minimum energy geometry very close to that of the $D_0$ state of $H_2O^+$, resulting in the photoionization process to be dominated by diagonal FC factors ($\Delta\nu$=0) [29]. This is consistent with the observations in the photoelectron kinetic energy distribution: a single peak located at the energetic limit (2.20 eV). The TRPES spectra were also measured at longer pump wavelengths where the two photon energies were insufficient for the excitation of the $\tilde{F}$ states [20, 29, 32–34]. Feature II observed at pump wavelength of 223.0 nm disappeared at these longer pump wavelengths, in support of the assignment of feature II at 223.0 nm pump wavelength to the $\tilde{F}$ states.

DOI:10.1063/1674-0068/cjcp1811243 

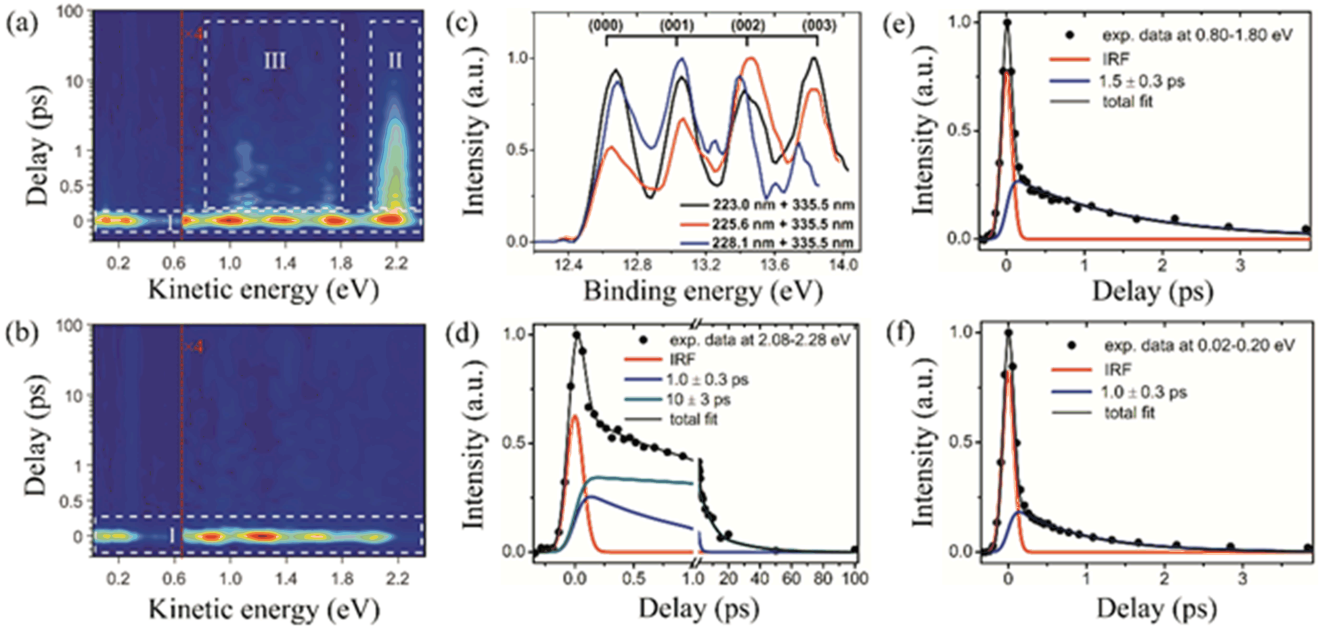


FIG. 2 (a,b) TRPES spectra of $H_2O$ at pump wavelengths of 223.0 and 225.6 nm, respectively. The background photoelectrons generated from single-color multiphoton ionization have been subtracted. (c) The binding energy distributions of photoelectron at pump wavelengths of 223.0, 225.6, and 228.1 nm. (d−f) Normalized transients for photoelectrons over kinetic energy ranges of 2.08−2.28, 0.80−1.80, and 0.02−0.20 eV, respectively. Solid dots show the experimental data, while the lines show the fits to the experimental data.

Feature III is well fitted by including a single exponential decay function, besides IRF presenting the contribution from feature I (FIG. 2(e)). The derived time constant is 1.5±0.3 ps. Feature III shows differences both in the time delay dependence and pump wavelength dependence, suggesting that it has a different source other than the $\tilde{F}$ states. However, the assignment of feature III is less clear-cut. We tentatively assign it to the excitation of lower electronic state(s), presumably vibrationally excited. The detailed analysis is out of the scope of the current study and no further discussion will be given.

The TRPES data for the $D_2O$ molecule, shown in FIG. 3(a), are fitted and analyzed in an analogous manner and lifetimes of 1.9±0.4 and 30±10 ps are derived for the two $\tilde{F}$ states, respectively.

### B. The decay mechanism of the $\tilde{F}$ states

The decay dynamics study of the $\tilde{F}$ states of water is lack. In a high resolution absorption spectroscopic study, the rotational lines of the $\tilde{F}^1B_1(0,0,0)\leftarrow\tilde{X}(0,0,0)$ band of $H_2O$ were partially resolved and a lifetime of 7−15 ps was estimated based on the linewidths of the rotational lines [35]. This is in very good agreement with one of the time constants derived from the current study, 10±3 ps. Therefore, the time constant of 10±3 ps is assigned to the lifetime of the $\tilde{F}^1B_1$ state, while 1.0±0.3 ps to the $\tilde{F}^1A_1$ state.

The $n$d components, $\tilde{D}''^1A_2$, $\tilde{E}^1B_1$, $\tilde{E}^1B_2$, $\tilde{F}^1A_1$ and $\tilde{F}^1B_1$ for 3d, are mutually coupled with each other through Coriolis interaction [36]. The two $\tilde{F}$ states show heavy similarities in many aspects of the potential energy surface [29]. The excitation energies of these two states are also virtually the same: the largest separation derived from various experimental and theoretical studies is only ∼60 meV [20, 29, 32–34]. It is, therefore, worthy of a detailed investigation on why the $\tilde{F}^1A_1$ state decays with a rate about one order of magnitude faster than the $\tilde{F}^1B_1$ state. In an *ab initio* configuration interaction calculation by Child and coworkers, the bending potential energy curves of Rydberg $^1A_1$, $^1A_2$, $^1B_2$ and $^1B_1$ states of $H_2O$ were derived [29]. In the manifold of $^1A_1$ Rydberg states, the 'bent' $\tilde{D}$ and 'linear' $\tilde{B}$ states are energetically lower than the $\tilde{F}^1A_1$ state. Strong configuration interaction between the $\tilde{D}$ and $\tilde{B}$ states results into a sharp avoided crossing between their potential energy curves. The resulting adiabatic potential energy curve of the $\tilde{D}$ state is strongly repulsive at small bent angles and nonadiabatic coupling between the $\tilde{D}$ and $\tilde{F}^1A_1$ states is expected, presumably caused by the bending mode (of $A_1$ symmetry). Therefore, we propose that the dominating decay channel of the $\tilde{F}^1A_1$ state is internal conversion (IC) to the $\tilde{D}$ state that is again strongly predissociated via the $\tilde{B}$ state [7, 8, 34]. A close inspection of the TRPES data (FIG. 2(a)) provides a direct evidence to this decay mechanism: there is a very weak, sharp peak at 0.1 eV. The time-delay dependence of this peak (integrated over 0.02−0.20 eV)

DOI:10.1063/1674-0068/cjcp1811243 

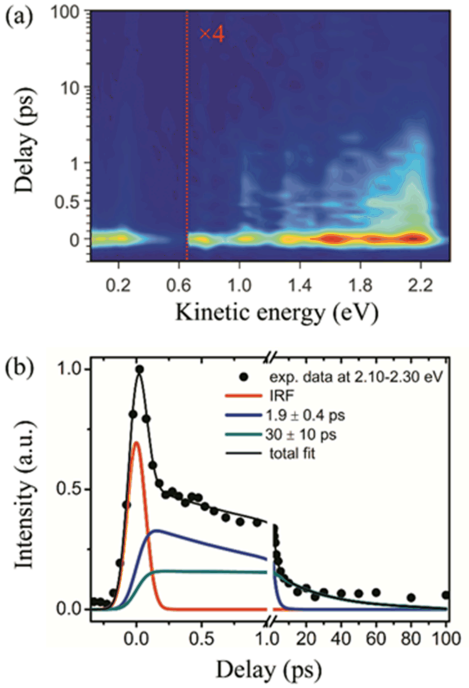


FIG. 3 (a) TRPES spectra of $D_2O$ at pump wavelengths of 222.6 nm. The background photoelectrons generated from single-color multiphoton ionization have been subtracted. (b) Photoelectron transient integrated over 2.10−2.30 eV. Solid dots show the experimental data, while the lines show the fits to the experimental data.

is shown in FIG. 2(f). It is fitted using Eq.(1) and a single exponential decay function is involved, besides the IRF accounting for the contribution from feature I. The fitting quality is satisfactory and the derived time constant is the same as that of the $\tilde{F}^1A_1$ state: 1.0±0.3 ps. The $\tilde{F}^1A_1$ state is dominated by the $3db_1 \leftarrow 1b_1$ configuration and mainly associated to $H_2O^+$ ($D_0$) upon photoionization. However, the $\tilde{D}$ state has a combination of $3pb_1 \leftarrow 1b_1$ and $3sa_1 \leftarrow 3a_1$ configurations due to the strong interaction with the $\tilde{B}$ state. As such, the $\tilde{D}$ state can be ionized to both the $D_0$ and $D_1$ states of $H_2O^+$. Therefore, the 0.1 eV peak is associated to photoionization of the $\tilde{D}$ state to $H_2O^+$ ($D_1$). The expected energy of photoelectron is 0.09 eV, calculated using the vertical excitation energy of $D_1$ (14.73 eV) [37], in perfect agreement with the experimental results. The lifetime of the $\tilde{D}$ state is much smaller than 1 ps [7, 8], rendering the time-delay dependence of photoelectron signal from the $\tilde{D}$ state resembles that of the $\tilde{F}^1A_1$ state itself. The decay mechanism proposed above is consistent with a recent study on the photodissociation dynamics of $H_2O$ [25]. In this study, it was found that the rotational and angular distributions of OH fragments after excitation at 111.5 nm are very similar to those for the $\tilde{B}$ state photodissociation and the authors suggested that the initial excited $\tilde{F}^1A_1$ state decays to the $\tilde{B}$ state, through a series of IC processes.

The lifetime of the $\tilde{F}^1B_1$ state is about an order of magnitude longer than that of the $\tilde{F}^1A_1$ state. The likely decay channel of the former is IC to the latter, caused by Coriolis interaction. In summary, the decay mechanisms of the $\tilde{F}$ states can be expressed as:

$$H_2O(\tilde{F}^1B_1) \xrightarrow{\text{Coriolis interaction}} H_2O(\tilde{F}^1A_1),$$
$$\tau_{\tilde{F}^1B_1}=10\pm3 \text{ ps}$$
$$H_2O(\tilde{F}^1A_1) \xrightarrow{\text{Nonadiabatic coupling}} H_2O(\tilde{D}^1A_1),$$
$$\tau_{\tilde{F}^1A_1}=1.0\pm0.3 \text{ ps}$$
$$H_2O(\tilde{D}^1A_1) \xrightarrow{\text{Configuration interaction}} H_2O(\tilde{B}^1A_1),$$
$$\tau_{\tilde{D}^1A_1}\ll 1 \text{ ps}$$

## IV. CONCLUSION

The ultrafast dynamics of water molecules excited to the $\tilde{F}$ states is studied by combining two-photon excitation and TRPEI techniques. The lifetimes of the $\tilde{F}^1A_1$ and $\tilde{F}^1B_1$ states of $H_2O$ ($D_2O$) were derived to be 1.0±0.3 (1.9±0.4) and 10±3 (30±10) ps, respectively. We propose that the $\tilde{F}^1A_1$ state mainly decays to $\tilde{D}$ state, through the nonadiabatic coupling between them, while the $\tilde{F}^1B_1$ state decays through the $\tilde{F}^1A_1$ state via the mutual Coriolis interaction. High-level theoretical work is demanded to verify the proposed decay mechanisms.

## V. ACKNOWLEDGEMENTS

This work was supported by the National Natural Science Foundation of China (No.21573228, No.21833003, No.21673232, and No.21773236) and the Strategic Priority Research Program of the Chinese Academy of Sciences (No.XDB17000000).

[1] S. Bell, J. Mol. Spectry. **16**, 205 (1965).
[2] M. N. R. Ashfold, J. M. Bayley, and R. N. Dixon, Chem. Phys. **84**, 35 (1984).
[3] A. Hodgson, J. P. Simons, M. N. R. Ashfold, J. M. Bayley, and R. N. Dixon, Mol. Phys. **54**, 351 (1985).
[4] K. J. Yuan, Y. A. Cheng, L. N. Cheng, Q. Guo, D. X. Dai, X. M. Yang, and R. N. Dixon, J. Chem. Phys. **133**, 134301 (2010).
[5] K. Yuan, R. N. Dixon, and X. Yang, Acc. Chem. Res. **44**, 369 (2011).
[6] X. Hu, L. Zhou, and D. Xie, WIREs Comput. Mol. Sci. **8**, 1350 (2018).
[7] O. Steinkellner, F. Noack, H. H. Ritze, W. Radloff, and I. V. Hertel, J. Chem. Phys. **121**, 1765 (2004).
[8] Z. G. He, D. Y. Yang, Z. C. Chen, K. J. Yuan, D. X. Dai, G. R. Wu, and X. M. Yang, Phys. Chem. Chem. Phys. **19**, 29795 (2017).

DOI:10.1063/1674-0068/cjcp1811243 

[9] S. Hennig, V. Engel, R. Schinke, and V. Staemmler, Chem. Phys. Lett. **149**, 455 (1988).
[10] V. Engel, V. Staemmler, R. L. Vanderwal, F. F. Crim, R. J. Sension, B. Hudson, P. Andresen, S. Hennig, K. Weide, and R. Schinke, J. Phys. Chem. **96**, 3201 (1992).
[11] M. Wittmann, M. T. Wick, O. Steinkellner, P. Farmanara, V. Stert, W. Radloff, G. Korn, and I. V. Hertel, Opt. Commun. **173**, 323 (2000).
[12] J. H. Fillion, R. van Harrevelt, J. Ruiz, N. Castillejo, A. H. Zanganeh, J. L. Lemaire, M. C. van Hemert, and F. Rostas, J. Phys. Chem. A **105**, 11414 (2001).
[13] E. Segev and M. Shapiro, J. Chem. Phys. **77**, 5604 (1982).
[14] R. N. Dixon, Mol. Phys. **54**, 333 (1985).
[15] H. J. Krautwald, L. Schnieder, K. H. Welge, and M. N. R. Ashfold, Faraday Discuss. **82**, 99 (1986).
[16] K. Weide and R. Schinke, J. Chem. Phys. **87**, 4627 (1987).
[17] A. H. Zanganeh, J. H. Fillion, J. Ruiz, M. Castillejo, J. L. Lemaire, N. Shafizadeh, and F. Rostas, J. Chem. Phys. **112**, 5660 (2000).
[18] Y. Cheng, K. Yuan, L. Cheng, Q. Guo, D. Dai, and X. Yang, J. Chem. Phys. **134**, 064301 (2011).
[19] R. N. Dixon, D. W. Hwang, X. F. Yang, S. Harich, J. J. Lin, and X. Yang, Science **285**, 1249 (1999).
[20] P. Gurtler, V. Saile, and E. E. Koch, Chem. Phys. Lett. **51**, 386 (1977).
[21] M. N. R. Ashfold, J. M. Bayley, R. N. Dixon, and J. D. Prince, Ber. Bunsen-Ges. Phys. Chem. Chem. Phys. **89**, 254 (1985).
[22] G. Meijer, J. J. Termeulen, P. Andresen, and A. Bath, J. Chem. Phys. **85**, 6914 (1986).
[23] K. Yuan, Y. Cheng, L. Cheng, Q. Guo, D. Dai, X. Wang, X. Yang, and R. N. Dixon, Proc. Natl. Acad. Sci. **105**, 19148 (2008).
[24] K. J. Yuan, L. N. Cheng, Y. Cheng, Q. Guo, D. X. Dai, and X. M. Yang, J. Chem. Phys. **131**, 074301 (2009).
[25] H. Wang, Y. Yu, Y. Chang, S. Su, S. Yu, Q. Li, K. Tao, H. Ding, J. Yang, G. Wang, L. Che, Z. He, Z. Chen, X. Wang, W. Zhang, D. Dai, G. Wu, K. Yuan, and X. Yang, J. Chem. Phys. **148**, 124301 (2018).
[26] Z. G. He, Z. C. Chen, D. Y. Yan, D. X. Dai, G. R. Wu, and X. M. Yang, Chin. J. Chem. Phys. **30**, 247 (2017).
[27] V. Dribinski, A. Ossadtchi, V. A. Mandelshtam, and H. Reisler, Rev. Sci. Instrum. **73**, 2634 (2002).
[28] S. Y. Truong, A. J. Yencha, A. M. Juarez, S. J. Cavanagh, P. Bolognesi, and G. C. King, Chem. Phys. **355**, 183 (2009).
[29] D. M. Hirst and M. S. Child, Mol. Phys. **77**, 463 (1992).
[30] T. Koopmans, Physica **1**, 104 (1934).
[31] Y. Wu and V. S. Batista, J. Phys. Chem. B **106**, 8271 (2002).
[32] R. D. Gilbert, M. S. Child, and J. W. C. Johns, Mol. Phys. **74**, 473 (1991).
[33] W. A. Goddard and W. J. Hunt, Chem. Phys. Lett. **24**, 464 (1974).
[34] R. van Harrevelt and M. C. van Hemert, J. Chem. Phys. **112**, 5777 (2000).
[35] P. L. Smith, K. Yoshino, H. E. Griesinger, and J. H. Black, Astrophys. J. **250**, 166 (1981).
[36] M. S. Child and C. Jungen, J. Chem. Phys. **93**, 7756 (1990).
[37] G. H. F. Diercksen, W. P. Kraemer, T. N. Rescigno, C. F. Bender, B. V. McKoy, S. R. Langhoff, and P. W. Langhoff, J. Chem. Phys. **76**, 1043 (1982).

DOI:10.1063/1674-0068/cjcp1811243 